# Models

We propose several models which include differents rotational velocities and optical depths. We also take into account the dust within the gas and two differents initial distributions of the photons, central and homogeneous. At the end we study 48 models, those are resumed in Table[1]

| | |
|---|---|
| Velocity(km/s) | 50, 100, 200, 300 |
| Optical Depth | $\tau = 10^5, 10^6, 10^7$ |
| Photons Distributions | Central, Homogeneous |

Table 1: Models, If we take into account all these possibles combinations we get 24 models with dust and 24 without dust for a total of 48 models.

We later study this models taking into account the posititon of the observer respect to the axis of rotation of the cloud.

## Rotational Effect

Due to the resonant nature of the lyman alpha line, gas kinematics play an important role in the shape of this line. In particular we study the case in which this gas is spherically symmetric and its rotating.

In cartesian coordinates the rotational velocity around de the z-axys is defined by:

$$v_x = -\frac{y}{R}v \tag{1a}$$

$$v_y = \frac{x}{R}v \tag{1b}$$

Where $x$ and $y$ define de position of the gas atoms and dust particles. The minus sign in the x-component of the velocity is due to the direction of rotation, in this case we assume that as seeing from the top,the rotation is anticlockwise.

In Figure[1] the effect that rotation have in the spectra is shown, for both distributions central (Left) and homogeneous (right). This is a general case in the sense that is independent of the position of an external observer.

Figure 1: Shape of the lyman alpha line for differents velocities. The left panel show the central distribution while the right panel show the homogeneous distribution.

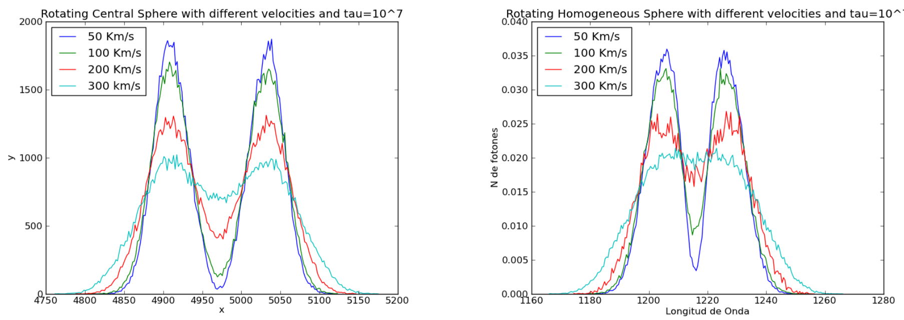


Now if we take into account the position of the observer and compute this for differents angles of observation $\theta$ the outcoming spectra is modified as is shown in figure[2]. The main feature here is that as the angle increases the line high decreases. It means that a observer in the poles will observe a higher double peak than a observer in the ecuator. We will understand this in more details when we present the resaults of the scape fraction in section[].

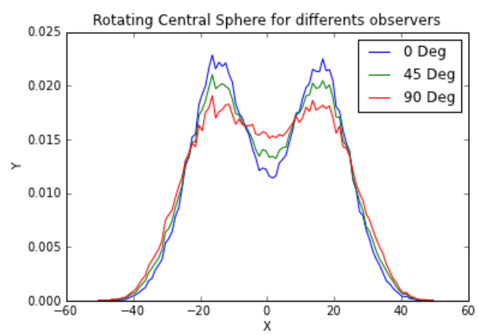


Figure 2: Spectra for different observers. Model:$V = 300 km/s$, Optical Depth $\tau = 10^7$ and Central Distribution without dust.

# Resaults and Discussion

In the previous section we describe the models that we study the effect of rotation in the Lyman alpha line and see the effect of rotation in the specrtums. Now we show the main resaults that we obtain, in particual we pay spetial attention to the position of the maximums, the width of the line and the escape fraction in function of the rotational velocity and the angle of observation $\theta$.

## Maximums Position

Figure 3: Width of the lyman-alpha line for all the models.

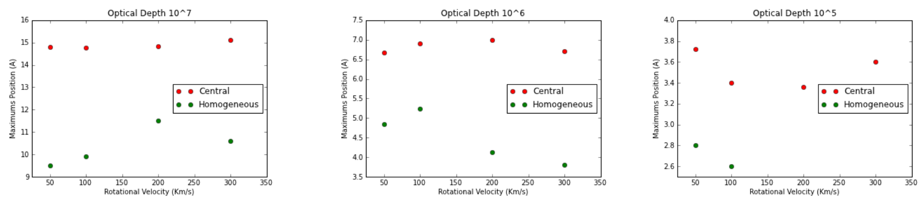


(comparar con la grafica del apendice de clara con el eje x el optical depth y en el eje-y los maximos)

The maximus position gives information about the wave lenght of the mayority of the outcoming photons after they interact with the gas, in addition as a photon have more scatterings its wave lenght would be larger than the initial which is 1216 Å. As we can see in Fig.[3] the position of the maximums does not change with rotational velocity. But it change from homogeneous and central.

## Line Width

Another effect that the rotation of the gas produce is in the width of the lyman alpha line. The width of the line provide information of the the how many phtons scape with a particular wave lenght, in the ideal case in which all the photons scape with the same wave lenght the outcoming spectrum would be narrow. For all the models we study we found that as the rotational velocity increase as the line width increase this is show in Fig.[4].

Figure 4: Width of the lyman-alpha line for all the models.

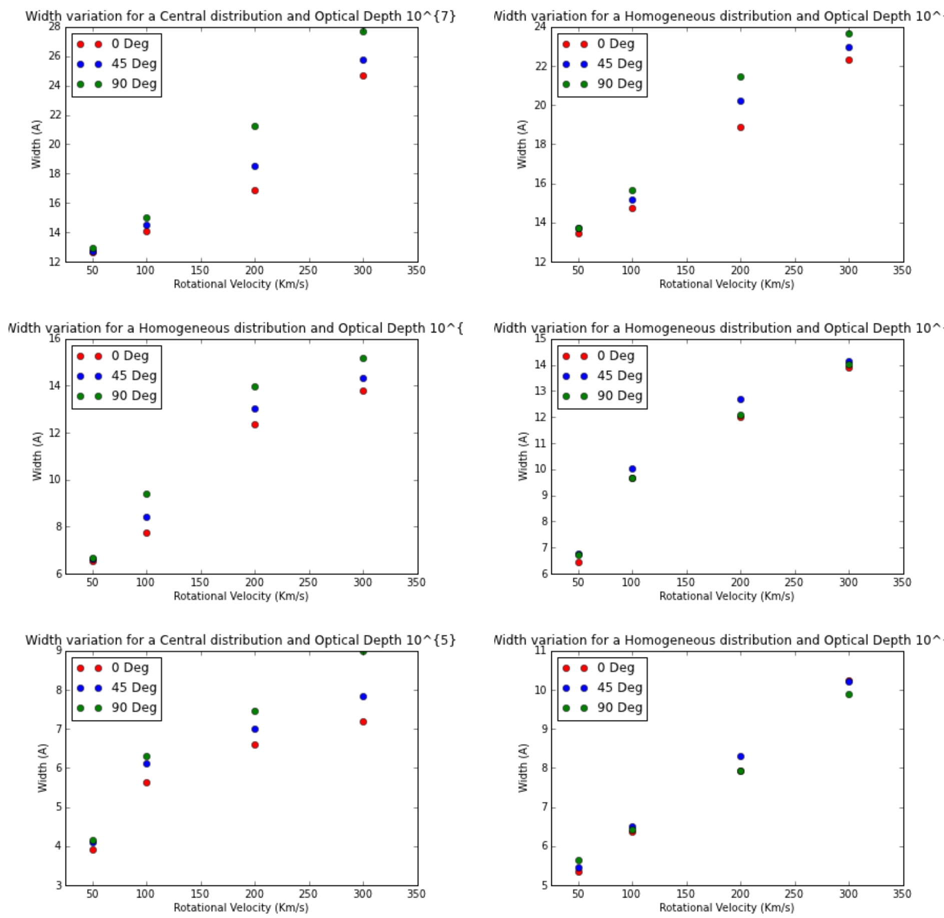


We also found that the width for a particular model is not the same for differents angles of observation in particular as the angle increase the width also increase, it means that as the angle increase the number of scatterings of the photons increasse for this reason we see a broader line. Fig.[5]

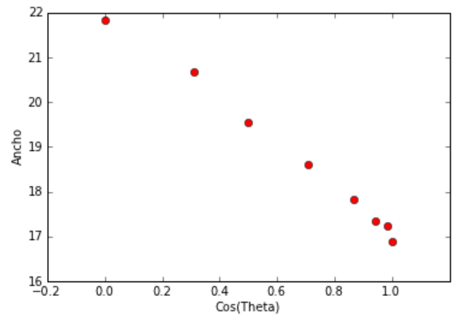


Figure 5: Width variation in function of theta

## Escape Fraction

The fraction of photons that escape from de cloud of gas and dust is defined as:

$$F_e = \frac{\Sigma_{NI}\vec{k} \cdot \vec{o}}{\Sigma_{NF}\vec{k} \cdot \vec{o}} \tag{2}$$

Where NI is the initial number of photons and NF is the final. This escape fraction is computed for all the models which resaults are shown in Fig.[6]

Figure 6: Escape fraction for all the models. Left panels show the central distribution, while right panels show the homogeneous distribution

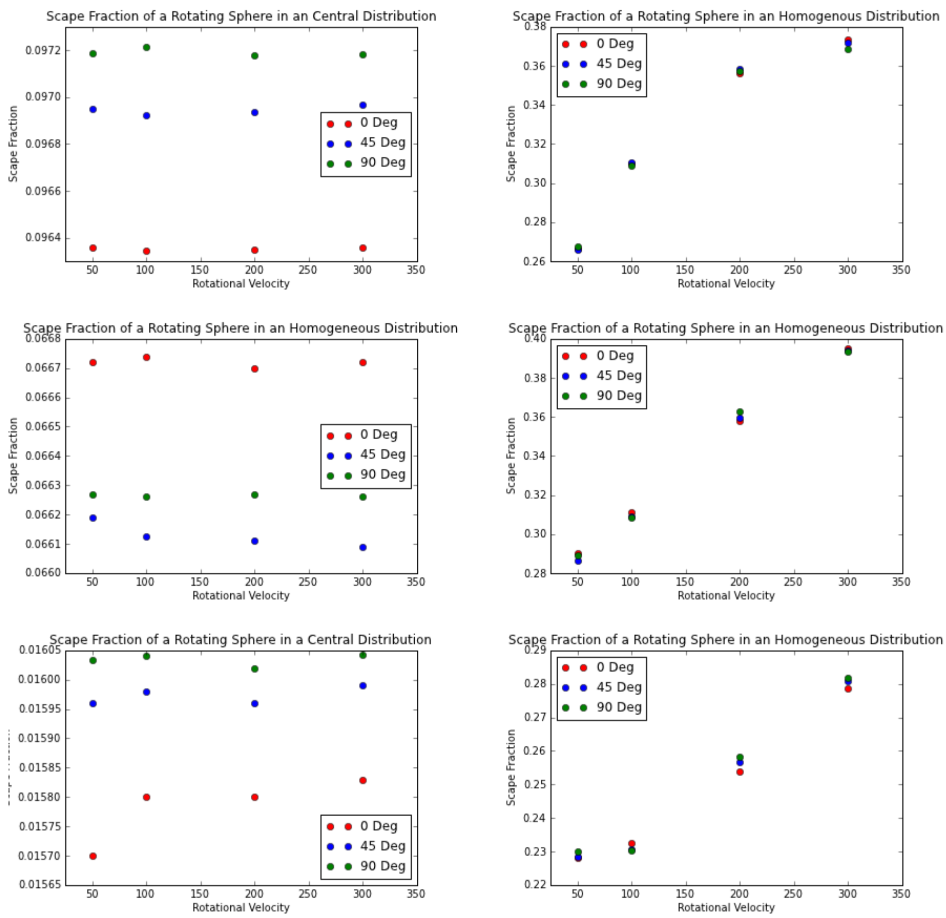


When the distribution is homogeneous the effect of velocity in the escape fraction is clear while in the central model the effect is not noterous. The main effect is that the escape fraction increase as the velocity increase.

# Observational effect.

# Tables

Maximos

| Velocity (Km/s) | Maximum 1 position | Maximum 2 position |
|---|---|---|
| 50 | -16.2695 | 16.23705 |
| 100 | -15.66496 | 15.33504 |
| 200 | -16.93149 | 14.56851 |
| 300 | -13.40048 | 16.09952 |

Table 2: Optical Depth $\tau = 10^7$, Central Distribution

| Velocity (Km/s) | Maximum 1 position | Maximum 2 position |
|---|---|---|
| 50 | -7.46286 | 6.53714 |
| 100 | -7.53357 | 6.96643 |
| 200 | -8.17453 | 7.32547 |
| 300 | -6.81487 | 6.18513 |

Table 3: Optical Depth $\tau = 10^6$, Central Distribution

| Velocity(Km/s) | Maximum 1 position | Maximum 2 position |
|---|---|---|
| 50 | -4.33708 | 3.66292 |
| 100 | -4.27326 | 3.72674 |
| 200 | -3.7737 | 3.7263 |
| 300 | -3.84903 | 4.15097 |

Table 4: Optical Depth $\tau = 10^5$, Central distribution

Line width

| Velocity(Km/s) | FWHM | $\theta$ |
|---|---|---|
| 50 | 12.62 | $0^o$ |
| 50 | 12.72 | $45^o$ |
| 50 | 12.93 | $90^o$ |
| 100 | 14.07 | $0^o$ |
| 100 | 14.48 | $45^o$ |
| 100 | 15.00 | $90^o$ |
| 200 | 16.90 | $0^o$ |
| 200 | 18.51 | $45^o$ |
| 200 | 21.24 | $90^o$ |
| 300 | 24.69* | $0^o$ |
| 300 | 25.79* | $45^o$ |
| 300 | 27.73* | $90^o$ |

Table 5: Lines Widhts for a Central Distribution and $\tau = 10^7$

Scape fracton

| Model | Velocity (km/s) | $\theta$ | Dust $\sum(s)$ | $\sum(s)$ |
|---|---|---|---|---|
| Homogeneous | 50 | $0^o$ | 13293.06 | 49939.53 |
| Homogeneous | 50 | $45^o$ | 13291.04 | 50001.59 |
| Homogeneous | 50 | $90^o$ | 13348.76 | 49922.73 |
| Homogeneous | 100 | $0^o$ | 15527.69 | 50114.11 |
| Homogeneous | 100 | $45^o$ | 15511.56 | 49967.17 |
| Homogeneous | 100 | $90^o$ | 15401.71 | 49833.65 |
| Homogeneous | 200 | $0^o$ | 17830.85 | 50078.69 |
| Homogeneous | 200 | $45^o$ | 17932.87 | 50064.42 |
| Homogeneous | 200 | $90^o$ | 17830.85 | 49931.748 |
| Homogeneous | 300 | $0^o$ | 18687.33 | 50048.33 |
| Homogeneous | 300 | $45^o$ | 18572.12 | 49922.67 |
| Homogeneous | 300 | $90^o$ | 18421.79 | 49979.37 |

Table 6: Escape fraction for a Homogeneous Distribution and optical depth $10^5$.

| Model | Velocity (km/s) | $\theta$ | Dust $\sum(s)$ | $\sum(s)$ |
|---|---|---|---|---|
| Central | 50 | $0^o$ | 4809.881 | 49917.069 |
| Central | 50 | $45^o$ | 4829.21 | 49811.79 |
| Central | 50 | $90^o$ | 4845.108 | 49853.039 |
| Central | 100 | $0^o$ | 4809.665 | 49921.30 |
| Central | 100 | $45^o$ | 4828.65 | 49820.13 |
| Central | 100 | $90^o$ | 4846.45 | 49854.0 |
| Central | 200 | $0^o$ | 4809.63 | 49917.64 |
| Central | 200 | $45^o$ | 4829.25 | 49818.49 |
| Central | 200 | $90^o$ | 4844.89 | 49856.66 |
| Central | 300 | $0^o$ | 4810.56 | 49922.98 |
| Central | 300 | $45^o$ | 4831.16 | 49823.33 |
| Central | 300 | $90^o$ | 4845.33 | 49858.48 |

Table 7: Escape fraction for the central Distribution and optical depth $10^5$.